INTERNATIONAL JOURNAL OF OPTIMIZATION IN CIVIL ENGINEERING
Int. J. Optim. Civil Eng., 2016; 6(2):227-243

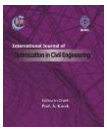

OPTIMUM DESIGN OF DOUBLE CURVATURE ARCH DAMS USING A QUICK HYBRID CHARGED SYSTEM SEARCH ALGORITHM

S. Talatahari[*, †], M.T. Aalami and R. Parsiavash
Department of Civil Engineering, University of Tabriz, Tabriz, Iran

ABSTRACT

This paper presents an efficient optimization procedure to find the optimal shapes of double curvature arch dams considering fluid–structure interaction subject to earthquake loading. The optimization is carried out using a combination of the magnetic charged system search, big bang-big crunch algorithm and artificial neural network methods. Performing the finite element analysis during the optimization process is time consuming. Back propagation neural network is utilized to reduce the computational burden. A real-world arch dam is considered as a numerical example to demonstrate the efficiency of the proposed method. The numerical results reveal the computational advantages of the new method for optimal design of arch dams.

Keywords: magnetic charged system search; big bang-big crunch; double curvature arch dam; optimum design; dam-reservoir interaction; neural networks.

Received: 14 September 2015; Accepted: 20 November 2015

1. INTRODUCTION

In recent years, there has been an increasing interest to find optimal designs of double curvature arch dams. Generally, optimization of an arch dam involves obtaining a scheme with minimum concrete volume while it is subjected to behavioral, geometric and stability constraints. This process needs high computational cost from both structural and optimization point of view.

An arch dam has a complicated geometry. Besides, fluid-structure interaction has significant effect in stress distribution on it. Structural dynamic analysis of an arch dam subjected to earthquake loading requires time-consuming finite element analysis. In recent

[*]Corresponding author: Department of Civil Engineering, University of Tabriz, Tabriz, Iran
[†]E-mail address: Talatahari@tabrizu.ac.ir (S. Talatahari)

studies, to avoid the complexity of the problem some simplifications are involved. In the number of studies, the arch dam is considered with empty reservoir [1, 2] and in some others reservoir's effect is simplified by added mass approach [3, 4] which overestimates the hydrodynamic effects in the dam body [5].

In addition to structural computational burden, optimization of the arch dam may also need thousands of fitness function evaluations by performing a FE analysis of the dam at each evaluation. This proves the necessity of presenting a robust methodology, which not only is effective but also needs least computational efforts. To date, some researches have been carried out using a combination of optimization and neural networks to find the optimal shape of arch dams with empty reservoir and frequency constraints [2, 6]. Metaheuristics and neural networks are also utilized considering frequency instead of stress constraints for shape optimization of arch dams in [7].

The magnetic charged system search (MCSS) is a metaheuristic optimization technique which recently proposed by Kaveh et al. [8] and it is an improved version of the standard CSS [9]. In the MCSS, magnetic forces are considered in addition to electrical forces using the Biot-Savart law [10]. This additional force provides useful information for the optimization process and enhances the performance of the CSS algorithm [8]. The big bang-big crunch (BBBC) is another metaheuristic approach that is based on one of the theories of evolution of the universe with the same name [11].

The back propagation neural network (BPNN) is one of the artificial neural network (ANN) algorithms that was first introduced by Paul Werbos in 1974. In general, the BPNN is a supervised learning method that works by forwarding the output layer to the input layer in changing the weights. Furthermore, the BPNN works like humans in which learning is performed through examples and exercises in each layer of the ANN.

In this study, an efficient and robust methodology is presented to find the optimal shape of double curvature arch dams considering hydrodynamic effects resulting from dam-reservoir interaction under seismic loading. To reduce the computational time, the optimization task is performed using a hybridized MCSS, BBBC and BPNN method. BPNN is used as an alternative for the exact FE analyzer. The concrete volume of dam body is considered as the objective function and the geometrical parameters will be its design variables. The constraints are Willam-Warnke failure criterion for stress state as well as some geometric and stability constraints. The effectiveness of proposed methodology is then evaluated for a well-known benchmark arch dam and the results are compared to those of other meta-heuristic methods documented in literatures.

2. ARCH DAM OPTIMIZATION PROBLEM

2.1 Mathematical model and optimization variables

The optimization problem can formally be stated as follows:

Find: $$\boldsymbol{X} = [x_1, x_2, x_3, ..., x_n] \quad (1)$$

Minimize: $$Mer(\boldsymbol{X}) = f(\boldsymbol{X}) * f_{penalty}(\boldsymbol{X}) \quad (2)$$

Subject to:

$$\begin{aligned} & g_i(\boldsymbol{X}) \le 0, \quad i = 1,2,...,\mathrm{k} \\ & x_{i\min} \le x_i \le x_{i\max} \end{aligned} \tag{3}$$

where $\boldsymbol{X}$ is the vector of design variables, g_i is the ith constraint from k inequality constraints and $Mer(\boldsymbol{X})$ is the merit function; $f(\boldsymbol{X})$ is the objective function which generally is to minimize the construction cost of the dam. In Eq. (2), $f_{penalty}(\boldsymbol{X})$ is the penalty function which results from the violations of the constraints corresponding to the response of the arch dam. Also, $x_{i\min}$ and $x_{i\max}$ are the lower and upper bounds of design variable vector. Exterior penalty function method is employed to transform the constrained dam optimization problem into an unconstrained one as follows:

$$f_{penalty}(\boldsymbol{X}) = 1 + \gamma_p \sum_{i=1}^{k} \max(0, gj(\boldsymbol{X}))^2 \tag{4}$$

where γ_p is the penalty multiplier.

A combination of concrete volume and casting area of dam body can be considered as the objective function [6]. However, since the variation of casting area between various designs is negligible (about one percent), it can be omitted in optimization process. So in this study, just the concrete volume of the dam is considered as the objective function:

$$v(\boldsymbol{X}) = \iint_A \left| y_u(x,z) - y_d(x,z) \right| dA \tag{5}$$

in which A is an area produced by projecting the dam body on a xz plan; $y_u(x,z)$ and $y_d(x,z)$ are parabolas of upstream and downstream surfaces of the arch dam, respectively. As shown in Fig. 1, the shape of the horizontal section of a parabolic arch dam is determined by these two parabolas as follows [12, 13]:

$$y_u(x,z) = \frac{x^2}{2r_u(z)} + g(z) \tag{6}$$

$$y_d(x,z) = \frac{x^2}{2r_d(z)} + g(z) + t_c(z) \tag{7}$$

where $r_u(z)$ and $r_d(z)$ are radius of curvature for upstream and downstream curves and $t_c(z)$ is thickness of crown cantilever at z direction, respectively. By dividing the dam height into n segments ($n+1$ controlling levels) and specifying the r_{ui}, r_{di} and t_{ci}, which denote the related values of the r_u, r_d and t_c at controlling levels, these values can be interpolated according to following equations of the nth order:

$$r_u(z) = \sum_{i=1}^{n+1} L_i(z)\, r_{ui} \tag{8}$$

$$r_d(z) = \sum_{i=1}^{n+1} L_i(z)\, r_{di} \tag{9}$$

$$t_c(z) = \sum_{i=1}^{n+1} L_i(z)\, t_{ci} \tag{10}$$

where, $L_i(z)$ is a Lagrange interpolation formula:

$$L_i(z) = \prod_{\substack{m=1 \\ m \neq i}}^{n+1} \frac{z - z_m}{z_i - z_m} \tag{11}$$

In Eqs. **Error! Reference source not found.** and **Error! Reference source not found.**, $g(z)$ is a polynomial of second order to define the curve of upstream boundary of crown cantilever (Fig. 2) and is determined as follow:

$$g(z) = \frac{\gamma}{2\beta h} z^2 - \gamma z \tag{12}$$

where $\gamma = \cot\alpha$ is slope of overhang at crest, *h* is dam height and the point where the slope of the upstream face equals to zero is $z = \beta h$.

2.2 Design variables

The most effective parameters for creating the arch dam geometry were mentioned in Section 2.1. These parameters can be adopted as design variables, as:

$$\boldsymbol{X} = \{\gamma \quad \beta \quad tc_1 \ldots tc_{n+1} \quad ru_1 \ldots ru_{n+1} \quad rd_1 \ldots rd_{n+1}\} \tag{13}$$

in which $\boldsymbol{X}$ contains $2+3(n+1)$ shape parameters of arch dam where, *n* is number of divisions along the dam height.

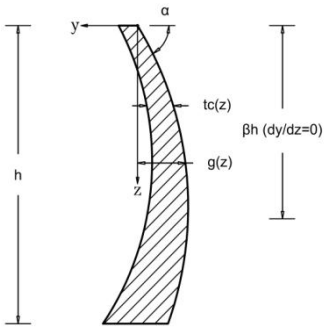

Figure 1. Crown Cantilever profile of the arch dam

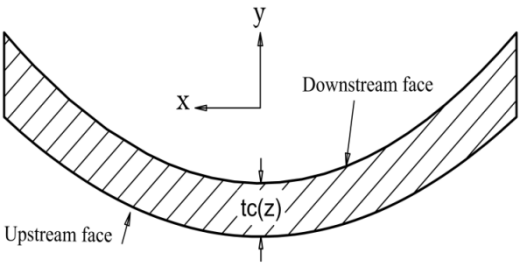

Figure 2. Parabolic shape of an elevation of the arch dam

2.3 Design constraints

Design constraints are divided into some groups including the behavioral, geometrical and stability constraints. In most of the existing studies, the separate restrictions of the principal stresses were considered as the behavior constraints. In this study, the behavior constraints are defined to prevent the crash and crack of each element (*e*) of the arch dam under specified safety factor (sf) in all time steps of a specified earthquake. For this purpose, the Willam and Warnke [14] failure criterion of concretes due to a multi-axial stress state is employed. Thus, time dependent (*t*) behavior constraints for the dam body are expressed as:

$$\left(\frac{F}{f_c}\right)_{e,t} \le \left(\frac{S}{s_f}\right)_{e,t} \Rightarrow gbe(x,t) = \left(\frac{F}{f_c} - \frac{S}{s_f}\right)_{e,t} \le 0, e = 1,2,\ldots,n_e, t = 1,2,\ldots,T \tag{14}$$

where F is a function of the principal stress state $(\sigma_1 \ge \sigma_2 \ge \sigma_3)$ and S is the failure surface expressed in terms of principal stresses containing: uniaxial compressive strength of concrete (f_c); uniaxial tensile strength of concrete (f_t); and biaxial compressive strength of concrete (f_{cb}). In the above relationship, T is the earthquake duration. According to four principal stress states compression-compression-compression, tensile-compression-compression, tensile-tensile-compression and tensile-tensile-tensile, the failure of concrete is categorized into four domains. In each domain, independent functions describe F and the failure surface, S. For instance, in the compression-compression-compression regime F and S are defined as:

$$F = \frac{1}{\sqrt{15}}\left[(\sigma_1 - \sigma_2)^2 + (\sigma_2 - \sigma_3)^2 + (\sigma_3 - \sigma_1)^2\right]^{\frac{1}{2}} \tag{15}$$

$$S = \frac{2r_2\left(r_2^2 - r_1^2\right)\cos\eta + r_2(2r_1 - r_2)\left[4\left(r_2^2 - r_1^2\right)\cos^2\eta + 5r_1^2 - 4r_1r_2\right]^{\frac{1}{2}}}{4\left(r_2^2 - r_1^2\right)\cos^2\eta + \left(r_{2\_} 2r_1\right)^2} \tag{16}$$

where the angle of similarity $0 \le \eta \le 60$ describes the relative magnitudes of the principal stresses as:

$$\cos\eta = \frac{2\sigma_1 - \sigma_2 - \sigma_3}{\sqrt{2}\left[(\sigma_1 - \sigma_2)^2 + (\sigma_2 - \sigma_3)^2 + (\sigma_3 - \sigma_1)^2\right]^{\frac{1}{2}}} \tag{17}$$

The parameters r_1 and r_2 represent the failure surface of all the stress states with $\eta = 0$ and $\eta = 60$, respectively, and these are functions of the principal stresses and concrete strengths (f_c, f_t, f_{cb}). The details of the failure criterion can be found in Ref. [14]. Therefore, Eq. (**Error! Reference source not found.**) is checked at the center of all dam elements (*ne*) for the earthquake loading [15]. If it is satisfied, there is no cracking or crushing. Otherwise, the material will crack if any principal stress is tensile, while crushing will occur if all principal stresses are compressive. The most important geometrical constraints are those that prevent from intersection of upstream face and downstream face, as:

$$r_{di} \le r_{ui} \Rightarrow \frac{r_{di}}{r_{ui}} - 1 \le 0, i = 1, 2, ..., (n+1) \tag{18}$$

where r_{di} and r_{ui} are the radii of curvatures at the down and upstream faces of the dam at *i*th level in the *z* direction, respectively and *n* is number of divisions along the dam height. The geometrical constraint applied to facilitate the construction is defined as:

$$\gamma \le \gamma_{alw} \Rightarrow \frac{\gamma}{\gamma_{alw}} - 1 \le 0 \tag{19}$$

where γ is the slope of overhang at the downstream and upstream faces of dam and γ_{alw} is its allowable value. Usually γ_{alw} is taken as 0.3, [13].

3. THE FINITE ELEMENT MODEL OF AN ARCH DAM

The Morrow Point double curvature arch dam is analyzed to assist the validation of the finite element model utilized in this study (Fig. 3). This dam has been studied by many researchers, so the results can be verified with already published material. This dam is located on the Gunnison River in Montrose Country near the village of Cimarron, Colorado. The dam has 142.65 m high and 220.68 m long along the crest and its thickness varies from 3.66 m at the crest to 15.85 m at the base level. The geometric properties of the dam in details can be found in [16]. The physical and mechanical properties involved here are the concrete density (2483 N.s2/m4), the concrete poison's ratio (0.2) and the concrete elasticity (27580 MPa). In this analysis, hydrodynamic effects of dam-reservoir interaction are considered. The dam body is discretized with two hundred and eighty 8-node solid elements

including 495 nodes for the dam body and one thousand and four hundred 8-node fluid element including 2145 nodes for the reservoir has been developed. This number of nodes and elements are not constant during the optimization process due to changes in dimensions of the arch dam and mesh generation in every analysis, so it will be varied when required. The arch dam is analyzed as a 3D-linear structure and the natural frequencies from the other literature and the present work are provided in Table 1. It can be observed that a good conformity has been achieved between the results of the present work with those of the reported in the literature.

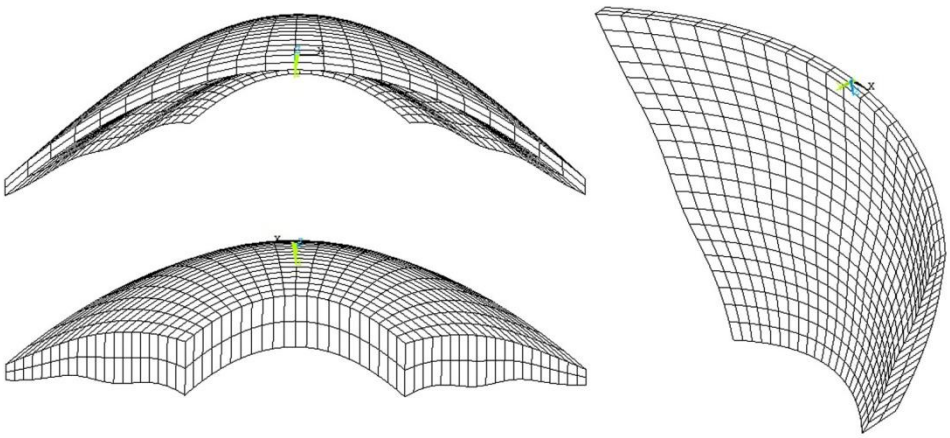

Figure 3. Finite element model of Morrow Point dam

Table 1: Comparison of the natural frequencies from the literature with FEM

mode	**(Tan and Chopra, 1996)**		**(Duron and Hall, 1988)**		**Present work**	
	Empty	Full	Full		Empty	full
	FEA		FEA	experimental	FEA	
1	4.27	2.82	3.05	2.95	4.2897	2.9607
2	-	-	-	3.3	-	3.3046
3	-	-	4.21	3.95	-	4.2425
4	-	-	5.96	5.4	-	4.9522
5	-	-	-	6.21	-	6.1156

4. UTILIZED ALGORITHMS

As mentioned before, in this paper, a powerful advanced algorithm are employed for optimal design of arch dams. Therefore, in the following part, we will firstly describe the standard and magnetic CSS-based methods as well as the BBBC and back propagation neural networks (BP); then the Quick Hybrid CSS (QHCSS) is introduced by combining these methods.

4.1 The standard charged search system

The CSS [9] is a population based search approach which is based on principles from physics and mechanics. The pseudo-code for the CSS algorithm can be summarized as follows [17]:

Step 1: *Initialization.* The initial positions of CPs are determined randomly in the search space and the initial velocities of CPs are assumed to be zero. The values of the fitness function for the CPs are determined and the CPs are sorted in an increasing order. A number of the first CPs and their related values of the fitness function are saved in a memory, so called Charged Memory (CM).

Step 2: *Determination of the forces on CPs.* The force vector is calculated for *j*th CP as:

$$\boldsymbol{F}_j = \sum_{i,i\neq j}\left(\frac{q_i}{a^3}r_{ij}\cdot i_1+\frac{q_i}{r_{ij}^2}\cdot i_2\right)ar_{ij}\,p_{ij}(\boldsymbol{X}_i-\boldsymbol{X}_j)\begin{cases}j=1,2,...,N\\ i_1=1,i_2=0\Leftrightarrow r_{ij}<a\\ i_1=0,i_2=1\Leftrightarrow r_{ij}\geq a\end{cases} \tag{20}$$

where F_j is the resultant force acting on the *j*th CP; $\boldsymbol{X}_i$ and $\boldsymbol{X}_j$ are the position vectors of the *i*th and *j*th CPs, respectively, Here a is the radius of the charged sphere and N is the number of CPs. p_{ij} is the probability of moving each CP towards the others and r_{ij} is the separation distance between two CPs. ar_{ij} indicates the kind of force. The magnitude of charge for each CP (q_i) is defined considering the quality of its solution as:

$$q_i=\frac{fit(i)-fitworst}{fitbest-fitworst},\qquad i=1,2,\ldots,N \tag{21}$$

where $fitbest$ and $fitworst$ are the best and the worst fitness of all particles, respectively; $fit(i)$ represents the fitness of the agent *i*; and N is the total number of CPs.

Step 3: *Solution construction.* Each CP moves to its new position and the new velocity is calculated as:

$$\boldsymbol{X}_{j,new}=rand_{j1}\cdot k_a\cdot\boldsymbol{F}_j+rand_{j2}\cdot k_v\cdot\boldsymbol{V}_{j,old}+\boldsymbol{X}_{j,old} \tag{22}$$

$$\boldsymbol{V}_{j,new}=\boldsymbol{X}_{j,new}-\boldsymbol{X}_{j,old} \tag{23}$$

where k_a is the acceleration coefficient; k_v is the velocity coefficient to control the influence of the previous velocity; and $rand_{j1}$ and $rand_{j2}$ are two random values uniformly distributed in the range (0,1).

Step 4: *Updating process.* If a new CP exits from the allowable search space, a harmony search-based handling approach is used to correct its position. In addition, if some new CP vectors are better than the worst ones in the CM; these are replaced by the worst ones in the CM.

Step 5: *Termination criterion control.* Steps 2-4 are repeated until a termination criterion

is satisfied, [9].

4.2 Magnetic charged system search algorithm

The main structure of the algorithm is the same as the standard CSS, but by some modification in part of the algorithm where the forces are computed. Thus, for considering this force in addition to electric force, the CSS is extended to the MCSS algorithm by Kaveh et al. [8]. In the MCSS algorithm, all steps described for the CSS are valid, yet; however, the relationship for the force affected on each CP should be modified considering the magnetic fields:

$$\boldsymbol{F} = p_r * \boldsymbol{F}_E + \boldsymbol{F}_B \tag{24}$$

where p_r is the probability that an electrical force is a repelling force. Here, $\boldsymbol{F}_E$ and $\boldsymbol{F}_B$ are the resultant electrical and magnetic forces, respectively. By using Eq. (**Error! Reference source not found.**), the resultant electrical force acting on the *j*th CP can be calculated, and the magnetic force $\boldsymbol{F}_{B,j}$ acting on the *j*th CP due to the magnetic field produced by the *i*th virtual wire (*i*th CP) can be expressed as:

$$\boldsymbol{F}_{\boldsymbol{B},j} = q_j . \sum_{i,i \neq j} \left(\frac{I_i}{R^2} r_{ij} . z_1 + \frac{I_i}{r_{ij}} . z_2 \right) . pm_{ji} . \left(\boldsymbol{X}_i - \boldsymbol{X}_j \right), \begin{cases} z_1 = 1, z_2 = 0 \Leftrightarrow r_{ij} < R, \\ z_1 = 0, z_2 = 1 \Leftrightarrow r_{ij} \geq R, \\ j = 1, 2, ..., N, \end{cases} \tag{25}$$

where R is the radius of the virtual wires, I_i is the average electric current in each wire, and pm_{ji} is the probability of the magnetic influence (attracting or repelling) of the *i*th wire (CP) on the *j*th CP and defined similar to the standard CSS. The average electric current in each wire I_i can be expressed as:

$$I_{avg,ik} = sign(df_{i,k}) * \frac{\left| df_{i,k} \right| - df_{\min,k}}{df_{\max,k} - df_{\min,k}}, \tag{26}$$

$$df_{i,k} = fit_k(\boldsymbol{X}_i) - fit_{k-1}(\boldsymbol{X}_i), \tag{27}$$

where $df_{i,k}$ is the variation of the objective function of the *i*th CP in the *k*th iteration.

4.3 Big bang-big crunch algorithm

The Big Bang-Big Crunch algorithm proposed by Erol and Eksin [11] which is based on the concept of the center of mass. Here, the term mass refers to the inverse of the fitness function value. The point representing the center of mass that is denoted by $\boldsymbol{X}_c$ is calculated according to the formula:

$$\boldsymbol{X}_c = \frac{\sum_{i=1}^{N} \frac{1}{fit(i)} \boldsymbol{X}_i}{\sum_{i=1}^{N} \frac{1}{fit(i)}} \tag{28}$$

where $\boldsymbol{X}_i$ is a point or candidate solution; N is the population size of the algorithm. When the Big Crunch phase is completed, the Big Bang phase is carried out to produce new candidates for the next iteration. These new candidates are produced using a normal distribution around the center of mass of the previous iteration. The standard deviation of this normal distribution decreases as the optimization process proceeds:

$$\boldsymbol{X}_{i,new} = \boldsymbol{X}_c + \frac{rand\,\alpha_1(\boldsymbol{X}_{\max} - \boldsymbol{X}_{\min})}{k+1} \qquad i = 1,2,...,n \tag{29}$$

where $\boldsymbol{X}_c$ stands for center of mass, *rand* is a normal random number, α_1 is a parameter limiting the size of the search space and k is the iteration step.

4.4 Hybrid MCSS and BBBC algorithm

In this new hybrid algorithm, the center of mass from the BBBC is added to the MCSS algorithm. In the other words, the new location of CPs is obtained as:

$$\mathbf{X}_{j,new} = rand_{j1} \cdot k_a \cdot \mathbf{F}_j + rand_{j2} \cdot k_v \cdot \mathbf{V}_{j,old} + rand_{j3} \cdot \mathbf{X}_c + \mathbf{X}_{j,old} \tag{30}$$

in which $rand_{j3}$ is a random value from [-1, +1]. In this hybrid algorithm, the positive advantages of the BBBC algorithm is added to the MCSS. In the other words, the new position of agents in the MCSS is obtained by using the forces generated by the other ones and this will guarantee a good exploration for the algorithm. However, applying the center of mass in addition to the above forces will enhance the exploitation ability of the algorithm. As a result, these two concepts will improve the performance of the algorithm without increasing the complexity of the method or required time for computations.

4.5 BP neural networks

The ANN is an engineering concept of knowledge in the field of artificial intelligence designed by adopting the human nervous system. One of the ANN algorithms called BPNN is a supervised learning method. It was first described by Paul Werbos in 1974 [18], and further developed by Rumelhart et al. in 1986 [19]. In general, the BPNN works by forwarding the output layer to the input layer in changing the weights. The layer in BPNN consists of three parts, namely input layer, hidden layer and output layer, Fig. 4. The basic backpropagation procedure for training the network is embodied in the following steps:

Step 1. Apply an input vector to the network and calculate the corresponding output values.

Step 2. Compare the actual outputs with the correct outputs and determine a measure of the error.

Step 3. Determine in which direction (+ or -) to change each weight in order to reduce the error.

Step 4. Determine the amount by which to change each weight.

Step 5. Apply the corrections to the weights.

Step 6. Repeat steps (1) through (5) with all the training vectors until the error for all vectors in the training set is reduced to an acceptable value.

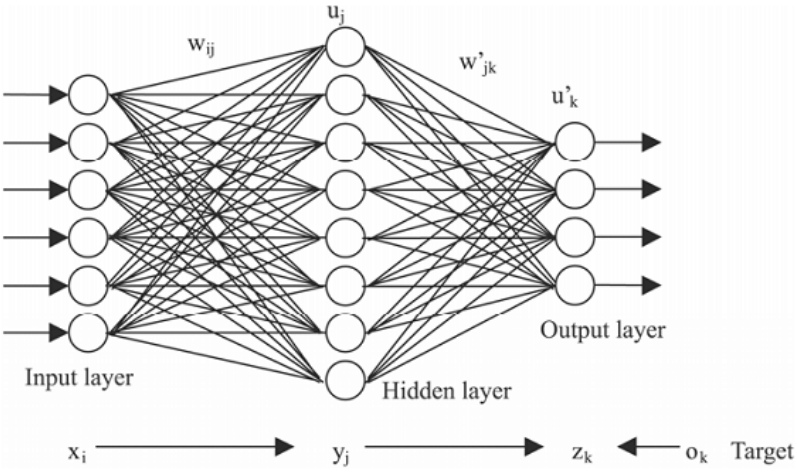

Figure 4. A typical structure of BPNN architecture

4.6 The proposed methodology

The Quick Hybrid CSS algorithm (QHCSS) is implemented as follows:

1. Initialize a number of random design of arch dams based on their geometric parameters and consider them as initial CPs.
2. Calculate principal stresses of each design (CP) using exact finite element analysis.
3. Calculate the maximum value of Willam-Warnke failure criterion among a time history results (called here MFC) for each dam.
4. Consider the geometric parameters of generated dams as the inputs and their corresponding MFC as the targets of BPNN.
5. Train BPNN using MATLAB.
6. Define the CM.
7. Determine both the electric and magnetic forces on CPs.
8. Perform solution construction.
9. Do position updating process.
10. Employ the trained BPNN for predicting the MFC of new CPs.
11. Evaluate the objective and constraint function by BPNN method.
12. Update CM.
13. Control termination criterion, if satisfied, stop otherwise go to the step (7).

5. NUMERICAL INVESTIGATION

5.1 Modeling and Softwares

To perform the optimization, the QHCSS algorithm is coded in MATLAB software; modeling and analyzing of the arch dam are performed using a combination of parallel working MATLAB and Ansys Parametric Design Language (APDL) codes. Reservoir is supposed to be full and the dam-reservoir interaction subjected to seismic loading is taken to account in this example. Since selection of any design earthquake will not affect the optimization process of the proposed methodology, the N–S record of 1940 El Centro earthquake is selected to apply to the arch dam-reservoir system in the upstream–downstream direction [20] as shown in Fig. 5. In order to construct the dam geometry, six controlling levels are considered so the dam can be modeled using twenty shape design variables:

$$\mathbf{X}=\{\gamma,\beta,\mathrm{t}_{c1},t_{c2},t_{c3},t_{c4},t_{c5},t_{c6},r_{u1},r_{u2},r_{u3},r_{u4},r_{u5},r_{u6},r_{d1},r_{d2},r_{d3},r_{d4},r_{d5},r_{d6}\} \tag{31}$$

In optimization process, we need the lower and upper bounds of design variables; these can be obtained using empirical design approaches, as [21]:

$$\begin{array}{lll} 0\le\gamma\le 0.3 & 0.5\le\beta\le 1 & \\ 3m\le t_{c1}\le 10m & 104m\le r_{u1}\le 135m & 104m\le r_{d1}\le 135m \\ 5m\le t_{c2}\le 14m & 91m\le r_{u2}\le 118m & 91m\le r_{d2}\le 118m \\ 7m\le t_{c3}\le 19m & 78m\le r_{u3}\le 101m & 78m\le r_{d3}\le 101m \\ 9m\le t_{c4}\le 23m & 65m\le r_{u4}\le 85m & 65m\le r_{d4}\le 85m \\ 11m\le t_{c5}\le 26m & 52m\le r_{u5}\le 68m & 52m\le r_{d5}\le 68m \\ 12m\le t_{c6}\le 31m & 39m\le r_{u5}\le 51m & 39m\le r_{d6}\le 51m \end{array} \tag{6}$$

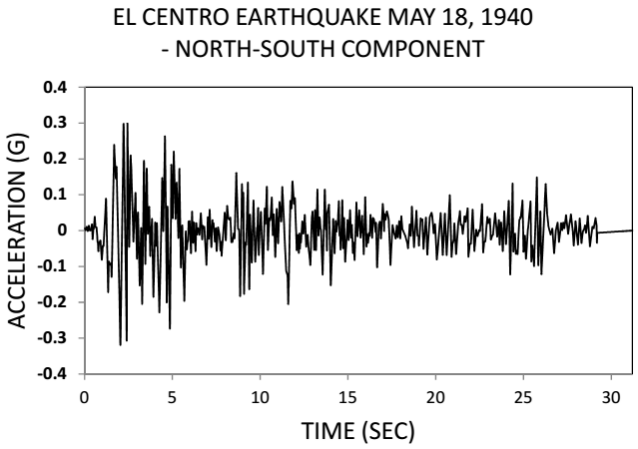

Figure 5. N–S record of 1940 El Centro earthquake

5.2 Neural network training and testing

For train and test the neural networks, inputs and outputs are the design variables of the arch dams and their corresponding MFC, respectively. Here, 300 training pairs are randomly generated and 210 and 90 samples are used for training and testing the network, respectively. Using the mentioned data BP neural network is trained. The time of training is 37 sec. The number of hidden layer neurons is set to 10. It should be noted that the number of BP neurons is determined by trial and error. In this case, the number of BP neurons is changed and the testing errors are monitored. The best results are observed in the case of 10 hidden layer neurons. The size of BP networks is 20-10-1. Figs. 6 and 7 show that the best performance of training and regression were 0.0038 and 0.9979, respectively. According to the results, the network has appropriate generalization and can be employed in the optimization process.

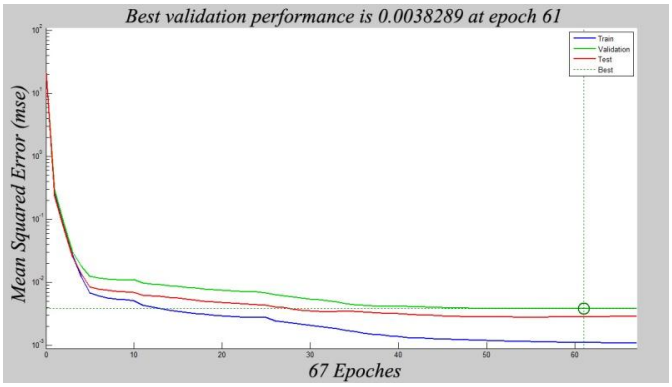

Figure 6. Plot result of BPNN performance

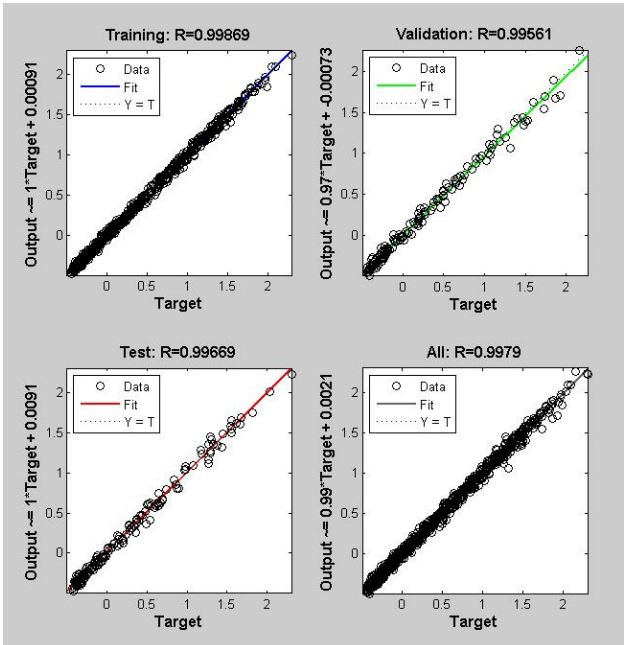

Figure 7. Plot result of BPNN regression

5.3 Results and discussion

The standard CSS, MCSS, and QHCSS are utilized in this paper to find optimum designs of dam structure. For the example presented in this paper, the number of agents is set to 50 and the number of iterations is limited to 200 for the all utilized algorithms. The other parameters for the new algorithm are as follows: $k_a = 2,\ k_v = 2,\ \alpha = 1$ and $k_t = 0.75$. Optimum solutions obtained by the various methods are provided in Table 2. This table proves that the QHCSS can find the optimum design of the dam very quick compared to the CSS and MCSS. Also, comparing the results show that this method can find better results than the other algorithms. The reason is on apply the center of mass concept in improving the performance of the algorithm.

Table 2: Optimum design of the arch dam obtained by different methods

	Kaveh et al. [22]			**Present work**				
Variable	PSO	CSS	CSS-PSO	CSS-FE	CSS-BP	MCSS-FE	MCSS-BP	QHCSS
$\gamma(m/m)$	0.1997	0.2183	0.2978	0.284	0.279	0.131	0.233	0.200
$\beta(m/m)$	0.9888	0.9744	0.9983	0.829	0.823	0.538	0.522	0.516
$tc_1(m)$	6.8690	6.2301	6.0086	7.114	7.373	5.507	5.0934	4.851
$tc_2(m)$	14.2055	15.0000	13.1002	7.696	7.666	11.085	10.069	8.973
$tc_3(m)$	17.5240	17.8633	15.2319	11.491	11.286	13.625	11.217	11.971
$tc_4(m)$	21.7109	20.5649	24.6122	17.701	16.963	15.293	16.776	16.298
$tc_5(m)$	23.5017	25.7853	20.0053	18.259	18.239	14.692	16.673	15.883
$tc_6(m)$	28.6766	26.9561	25.0028	31.109	31.157	14.630	18.331	16.891
$ru_1(m)$	133.9955	129.1776	133.4167	127.759	126.71	108.162	112.302	110.637
$ru_2(m)$	92.5018	109.5474	104.8836	98.522	98.919	93.785	94.273	93.582
$ru_3(m)$	99.9468	82.1169	87.4033	85.599	85.568	80.091	87.958	80.408
$ru_4(m)$	74.6562	70.8406	78.5695	82.919	83.064	68.396	68.074	67.689
$ru_5(m)$	50.6424	59.9997	53.6063	65.034	64.112	54.121	56.983	55.084
$ru_6(m)$	42.9266	40.3869	39.8787	45.490	44.872	40.291	41.563	41.713
$rd_1(m)$	112.3219	117.8332	101.8954	126.066	124.905	107.912	111.761	109.716
$rd_2(m)$	85.0033	85.5730	85.6888	97.223	96.5153	92.678	93.7835	92.719
$rd_3(m)$	70.6935	73.1176	70.2540	82.601	82.4507	80.3580	88.461	79.562
$rd_4(m)$	65.0838	64.2909	60.9596	70.348	69.8220	66.7040	67.907	66.340
$rd_5(m)$	50.5577	54.0687	52.1588	59.230	59.12868	53.9090	56.623	54.417
$rd_6(m)$	39.4978	35.5311	38.1512	40.587	40.17098	40.1450	40.679	39.994
Concrete volume (10^3 m^3)	3.49	3.47	3.36	2.49	2.46	2.34	2.32	2.24
Total elapsed time (min)	---	---	---	25960	652	26005	662	665

Also, Table 2 reveals that the solutions found in present work are much more better than that of results obtained by Kaveh et al. [22]. The difference comes from the superiority of the presented approach and the way of modeling the dam-reservoirs interaction. Kaveh et al. [21] used generalized Westergaard method for dam-reservoir interaction, which is an approximate method and overestimates the resulted stresses in dam body while in the present study exact finite element approach is used for this purpose.

It is observed that the overall time of optimization by neural networks including the data generation, network training and optimization task is significantly (0.025 times) less than that of optimization via full finite element analysis. Table 3 represents the MFC of optimum dams obtained by various methods mentioned in Table 2. The errors of approximate MFC of optimum designs predicted by BP network are compared to their corresponding accurate values obtained by exact analysis as shown in Table 4. It can be observed that the accuracy of approximate MFC obtained by BP is reasonably high. The present study demonstrates that the QHCSS creates a reliable and robust tool for arch-dam optimization for seismic loading.

Table 3: MFC of optimum dams obtained by different methods

	CSS		MCSS		QHCSS
	FE	BP	FE	BP	
MFC	-0.0669	-0.0644	-0.1100	-0.1118	-0.1393

Table 4: Error percentage of approximate MFC of optimum dams

Errors (%)	CSS-BP	MCSS-BP	QHCSS
Maximum errors			
Mean errors	0.0373	0.0163	0.0190

6. CONCLUSION

An efficient algorithm for shape optimization of double curvature arch dams is proposed in this paper. For this purpose, a finite element model of the arch dam-water system is presented and its performance is verified compared with the results reported in literature. Arch dam geometry is defined employing two polynomial for the central vertical section and two parabolas for the horizontal section. Concrete volume of dam body is considered as the objective function. By dividing the dam into five segments along the height, twenty design variables are considered as design parameters. In order to optimize the arch dam, a combination of the powerful optimization algorithms and neural networks are utilized. For this purpose, the magnetic CSS combined with BBBC and BBNN, so-called QHCSS, is presented. Maximum value of Willam Warnke failure criterion (MFC) is utilized as behavioral constraint to enforce resultant principal stresses to stay under a certain limit. Besides, some geometric and stability constraints are included. In order to reduce the computational cost of the optimization process, MFC of the arch dams are evaluated using properly trained back propagation (BP) neural network instead of their exact finite element

analysis. The proposed algorithms are applied to optimum design of Morrow Point dam as a well-known and real-world double curvature arch dam. In this example, the reservoir is assumed full and hydrodynamic effects of dam-reservoir interaction subjected to seismic loading are taken to account. Numerical results indicate that the approximate analysis-based optimization can significantly reduce the total computing time of FEA-based optimization while the errors are very small. Besides, the exact finite element method is more accurate and reliable approach for numerical modeling of the dam-reservoir interaction comparing the approximate added mass approach. The results also reveal that the QHCSS yields the best optimal solutions among other used methods.

REFERENCES

1. Kaveh A, Mahdavi VR. Optimal design of arch dams for frequency limitations using charged system search and particle swarm optimization, *Int J Optim Civil Eng* 2011; **4**: 543-555.
2. Gholizadeh S, Seyedpoor SM. Optimum design of arch dams with frequency limitations, *Int J Optim Civil Eng* 2011; **1**: 1-14.
3. Kaveh A, Mahdavi VR. Colliding bodies optimization for design of arch dams with frequency limitations, *Int J Optim Civil Eng* 2014; **4**: 473-490.
4. Akbari J, Ahmadi MT, Moharrami H. Advances in concrete arch dams shape optimization, *Appl Math Model* 2011; **35**: 3316-33.
5. Kuo JSH. Fluid-structure interactions: Added mass computations for incompressible fluid, in, Earthquake Engineering Research Center, University of California, Berkeley, 1982, pp. 126.
6. Kaveh A, Ghaffarian R. Shape optimization of arch dams with frequency constraints by enhanced charged system search algorithm and neural network, *Int J Civil Eng* 2014; **13**: 102-11.
7. Gholizadeh S, Seyedpoor SM. shape optimization of arch dams by metaheuristics and neural networks for frequency constraints, *Scientia Iranica* 2011; **18**: 1020-7.
8. Kaveh A, Motie Share MA, Moslehi M. Magnetic charged system search: a new meta-heuristic algorithm for optimization, *Acta Mech* 2013; **224**: 85-107.
9. Kaveh A, Talatahari S. A novel heuristic optimization method: charged system search, *Acta Mech* 2010a; 213: 267-89.
10. Halliday D, Resnick R, Walker J. *Fundamentals of Physics*, Wiley, New York, 2008.
11. Erol OK, Eksin I. A new optimization method: big bang–big crunch, *Adv Eng Softw* 2006; **37**: 106-11.
12. Zhu B. Shape optimization of arch dams, *Water Power & Dam Construction* 1987; **1**: 43-48.
13. Zhu B, Rao B, Jia J, Li Y. Shape optimization of arch dams for static and dynamic loads, *J Struct Eng* 1992; **118**: 2996-3015.
14. Willam KJ, Warnke EP. Constitutive model for the triaxial behavior of concrete, *In: International Association for Bridge and Structural Engineering,* 1975, pp. 1-30.
15. *USBR, Design criteria for concrete arch and gravity dams*, in: U.s.d.o.i.b.o. reclamation (Ed.), US Government Printing Office, Washington, 1977.

16. *USACE, Earthquake Design and Evaluation of Concrete Hydraulic Structures*, in, U. S. Army Corps of Engineers, Washington, D.C, America, 2007.
17. Kaveh A, Talatahari S. Optimal design of skeletal structures via the charged system search algorithm, *Struct Multidiscip Optim* 2010b; **41**: 893-911.
18. Werbos PJ. *Beyond Regression: New Tools for Prediction and Analysis in the Behavioral Sciences*, In, Harvard University, 1974.
19. Rumelhart D, Hinton G, Williams R. Learning representations by back-propagating errors, *Nature* 1986; 323: 533-6.
20. PEER, El Centro, 1940 Ground Motion Data, in: P.E.E.R. Centre (Ed.), 2009.
21. Varshney RS. *Concrete Dams*, 2 ed, Oxford and IBH Publishing Co, New Delhi, 1982.
22. Kaveh A, Mahdavi VR. Shape optimization of arch dams under earthquake loading using meta-heuristic algorithms, *KSCE J Civil Eng* 2013, **17**: 1690-9.